Forecasting Fire Season Severity in South America Using Sea Surface Temperature Anomalies

Yang Chen, *et al.*

Science **334**, 787 (2011);
DOI: 10.1126/science.1209472

18. J. K. Crouch, J. Suppe, *Geol. Soc. Am. Bull.* **105**, 1415 (1993).
19. N. McQuarrie, B. P. Wernicke, *Geosphere* **1**, 147 (2005).
20. D. S. Brothers *et al.*, *Nat. Geosci.* **2**, 581 (2009).
21. C. T. Herzig, D. C. Jacobs, *Geology* **22**, 991 (1994).
22. G. S. Fuis, W. D. Mooney, J. H. Healy, G. A. McMechan, W. J. Lutter, *J. Geophys. Res.* **89**, (B2), 1165 (1984).
23. T. Parsons, J. McCarthy, *Tectonics* **15**, 456 (1996).
24. A. Nicolas, *Nature* **315**, 112 (1985).
25. A. K. Schmitt, J. A. Vazquez, *Earth Planet. Sci. Lett.* **252**, 260 (2006).
26. R. L. Evans *et al.*, *Nature* **437**, 249 (2005).
27. M. P. Süss, J. H. Shaw, *J. Geophys. Res.* **108**, 2170 (2003).
28. S. E. Hansen, A. A. Nyblade, J. Julia, *S. Afr. J. Geol.* **112**, 229 (2009).
29. W. Buck, F. Martinez, M. S. Steckler, J. R. Cochran, *Tectonics* **7**, 213 (1988).
30. D. Wilson *et al.*, *Nature* **433**, 851 (2005).

Acknowledgments: This work was supported by the National Science Foundation EarthScope Program (EAR-0641772) and an EAR Postdoctoral Fellowship to V.L. (EAR-0948303). We thank the IRIS Data Management Center and the Southern California Earthquake Data Center for the waveform data used in this study. We thank H. Yuan, D. Forsyth, C. Rau, B. Schmandt, H. Ford, and D. Brothers for assistance with methods and interpretation.

Supporting Online Material

www.sciencemag.org/cgi/content/full/science.1208898/DC1
Materials and Methods
SOM Text
Figs. S1 to S10
References (*31*–*50*)

25 May 2011; accepted 26 September 2011
Published online 6 October 2011;
10.1126/science.1208898

Forecasting Fire Season Severity in South America Using Sea Surface Temperature Anomalies

Yang Chen,[1]* James T. Randerson,[1] Douglas C. Morton,[2] Ruth S. DeFries,[3] G. James Collatz,[2] Prasad S. Kasibhatla,[4] Louis Giglio,[5] Yufang Jin,[1] Miriam E. Marlier[6]

Fires in South America cause forest degradation and contribute to carbon emissions associated with land use change. We investigated the relationship between year-to-year changes in fire activity in South America and sea surface temperatures. We found that the Oceanic Niño Index was correlated with interannual fire activity in the eastern Amazon, whereas the Atlantic Multidecadal Oscillation index was more closely linked with fires in the southern and southwestern Amazon. Combining these two climate indices, we developed an empirical model to forecast regional fire season severity with lead times of 3 to 5 months. Our approach may contribute to the development of an early warning system for anticipating the vulnerability of Amazon forests to fires, thus enabling more effective management with benefits for climate and air quality.

Deforestation and forest degradation in South America contribute to anthropogenic carbon emissions and regional and global climate change (*1*–*4*). Fire is the dominant method for converting forest to cropland or pasture (*5*, *6*), and fires account for approximately half of the carbon emissions from deforestation and forest degradation in South America (*2*). Although deforestation rates in the Brazilian Amazon have declined over the past 5 years (*7*), trends in fires and burned area have not declined by the same amount, possibly because continued use of fire after deforestation maintains the risk of agricultural fires escaping into adjacent forests (*5*, *8*). Notably, extensive burning in the Brazilian states of Mato Grosso and Pará during 2007 led to the highest fire emissions of any year during the period 1997–2009 (*9*), highlighting the need to target forest degradation in addition to deforestation for sustained reductions in land use emissions from the region.

Projected decreases in Amazon rainfall during the 21st century (*10*, *11*) may increase the risk of forest fires (*12*), with the potential for larger carbon losses (*13*) and a positive feedback to climate change (*14*). Hence, the success of future climate mitigation and adaptation strategies will depend in part on more effective ways to manage fires. Advance information about the likelihood of fires in the dry season allows time to explore and implement management options such as allocation of firefighting resources or targeted burning restrictions.

[1]Department of Earth System Science, University of California, Irvine, CA 92697, USA. [2]NASA Goddard Space Flight Center, Biospheric Sciences Branch, Greenbelt, MD 20771, USA. [3]Department of Ecology, Evolution, and Environmental Biology, Columbia University, New York, NY 10027, USA. [4]Nicholas School of the Environment, Duke University, Durham, NC 27708, USA. [5]Department of Geography, University of Maryland, College Park, MD 20742, USA. [6]Department of Earth and Environmental Sciences, Columbia University, New York, NY 10027, USA.

*To whom correspondence should be addressed. E-mail: yang.chen@uci.edu

Table 1. Empirical fire model and validation statistics in different high-fire states in Brazil and Bolivia.

State	Peak fire month	Climate index–annual FSS relationship*				Empirical model†					Validation‡			
		Lead time (months)		*r*		Lead time	Model parameter			*r*	*r*			
		ONI	AMO	ONI	AMO		*a*	*b*	*c*	MOD	MYD	VIRS	ATSR	GFED3
Amazonas	September	10	4	0.28	0.72	4	0.72	53.2	13.8	0.72	0.68	0.61	0.08	0.52
Pará	August	3	4	0.57	0.80	3	46.4	281.2	144.1	0.88	0.68	0.72	0.55	0.54
Rondonia	September	7	4	0.62	0.88	4	86.8	1502	332.9	0.93	0.45	0.91	0.58	0.78
Mato Grosso	September	5	6	0.81	0.74	5	287.6	1101	483.9	0.92	0.76	0.74	0.69	0.74
El Beni	September	3	5	0.42	0.75	3	135.9	960.8	331.7	0.82	0.89	0.42	0.49	0.41
Acre	September	7	4	0.43	0.74	4	6.36	186.7	43.7	0.75	0.85	0.72	0.53	0.74

*Linear regressions between FSS (the annual sum of active fire counts during the fire season) recorded by Terra MODIS (MOD) and climate indices (either ONI or AMO) with different lead times (number of months prior to the peak fire month) were performed for 2001–2009. Maximum positive correlations (*r*) and associated lead times (with a cutoff of at least 3 months) are shown. Lead times are computed as the difference between the month of climate index and the peak fire month. Because the climate index is a 3-month mean SST anomaly, we report the lead time relative to the end of the 3-month climate index interval (not the center month) to give a more accurate description of the amount of time potentially available to develop a fire season severity forecast. †ONI and AMO values (2001–2009) that have maximum correlations with FSS were used to derive the empirical model using two-variable linear regressions; *a*, *b*, and *c* are coefficients of the formula (Eq. 1). The lead time describes the number of months before peak fire season for which the empirical model can be used for FSS prediction (and is the shorter of the two climate index lead times). *r* is the correlation between predicted and MODIS observed FSS for 2001–2009. ‡We validated the empirical model by comparing the predicted FSS with observed FSS from a different MODIS onboard the Aqua satellite (MYD, 2003–2010), the Visible and Infrared Scanner onboard the Tropical Rainfall Measuring Mission (TRMM) satellite (VIRS, 1998–2009), the European Space Agency (ESA) Advanced Along Track Scanning Radiometer World Fire Atlas (ATSR, 1997–2010, algorithm 1), and fire emissions from Global Fire Emission Database version 3 (GFED3, 1997–2009).

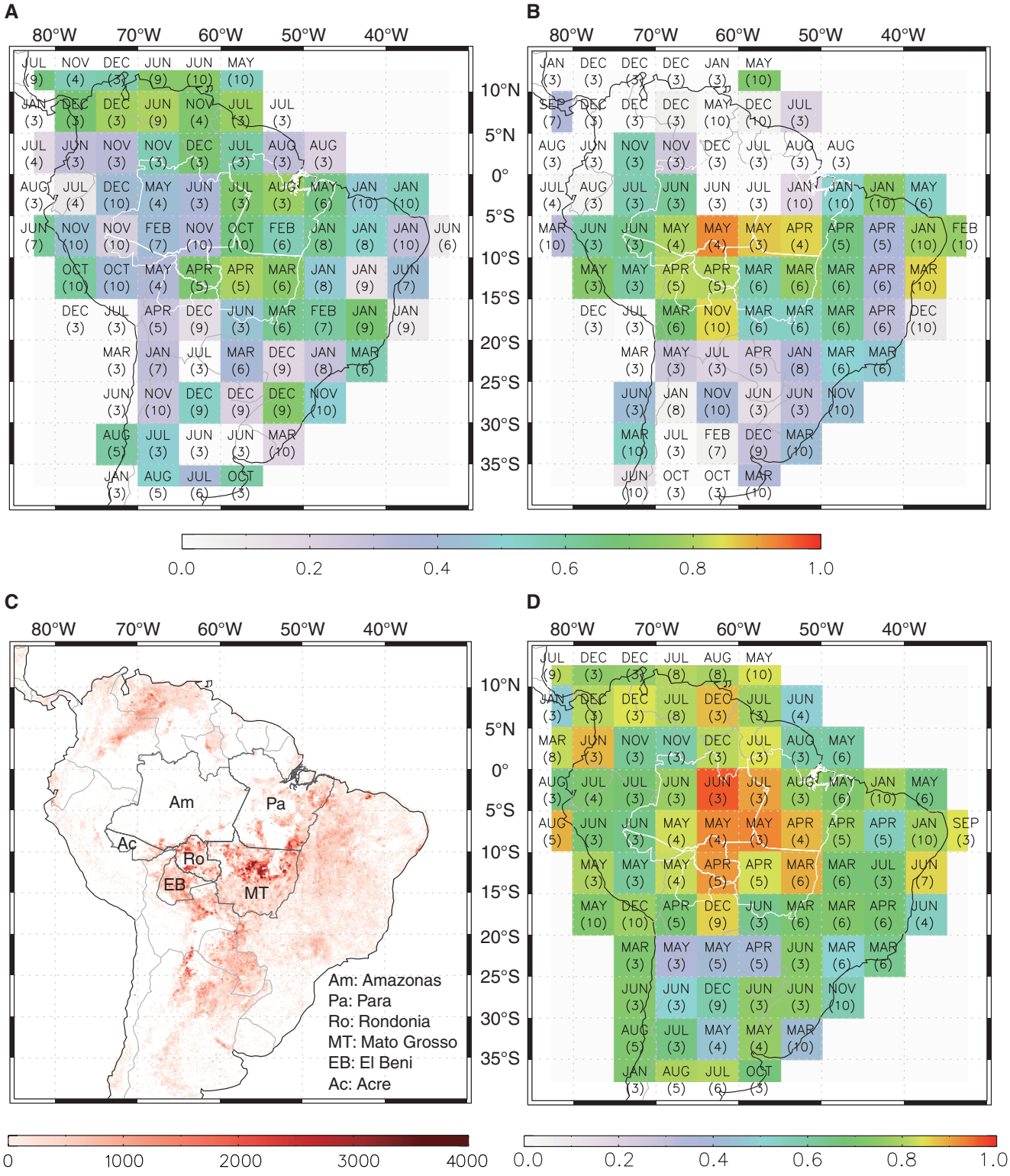

Fig. 1. (**A**) Maximum positive correlation between Oceanic Niño Index (ONI) and fire season severity (FSS) derived from 2001–2009 MODIS active fire data. (**B**) Maximum positive correlation between Atlantic Multidecadal Oscillation index (AMO) and FSS for the same period. (**C**) Mean FSS (in terms of detectable fires per million hectares per year) observed by MODIS during 2001–2009. (**D**) Correlation between predicted FSS from the empirical model (Eq. 1) and observed FSS derived from MODIS. ONI is a 3-month mean SST anomaly in the Niño 3.4 region (5°N to 5°S, 120° to 170°W) of the Pacific (*27*). AMO represents a similar 3-month mean for the North Atlantic (0° to 70°N) (*28*). The months at which ONI or AMO had largest positive correlation with FSS are provided for each 5° × 5° grid cell in (A) and (B). Also shown in the parentheses are the associated lead times (in months) relative to the peak fire month. The months (and the associated lead times) at which the empirical model can be used for FSS prediction are shown in (D). The spatial distribution of active fires across the Amazon shown in (C) is closely related to patterns of land use, including rates of forest clearing, the distribution of protected areas, and transportation corridors (*2*, *6*, *8*, *13*).

We developed a predictive relationship between sea surface temperature (SST) anomalies and annual fire season severity (FSS) in South America that enables forecasts with lead times of 3 to 5 months. A recent study (*15*) has shown that anomalous local fire activity in the western Amazon can be forecast using SSTs from the tropical North Atlantic. Our approach builds on this work by combining information from both the Pacific and Atlantic and by allowing for spatially varying contributions from these two different drivers across the continent. With our model, we were able to successfully predict interannual variability in FSS for several regions. Examination of the temporal and spatial variability of the model parameters and lead times provided additional information about the underlying mechanisms enabling these predictions.

High-fire years in South America are often associated with an extended dry season and anomalously low levels of precipitation (*16*–*18*). Previous studies [e.g., (*19*–*21*)] have shown that precipitation variability in the Amazon is regulated by SSTs in both the Pacific and Atlantic. During the warm phase of El Niño–Southern Oscillation (ENSO), precipitation is suppressed over the central and eastern Amazon (*22*, *23*). Atlantic SSTs also contribute to precipitation variability within the Amazon. Anomalously warm SSTs over the tropical North Atlantic are believed to cause a northward displacement of the Intertropical Convergence Zone (ITCZ), which in turn decreases convection and precipitation during the dry season in the western and southwestern Amazon (*24*). Thus, the most severe droughts observed in the Amazon over the past three decades have occurred when the tropical eastern Pacific and North Atlantic were anomalously warm (*16*–*18*, *24*, *25*).

Fire season severity, here defined as the sum of satellite-based active fire counts in a 9-month period centered at the peak fire month, depends on multiple parameters that influence fuel moisture levels and fire activity in addition to precipitation, including vapor pressure deficits, wind speeds, ignition sources, land use decisions, and the duration of the dry season. As a result, the relationship between FSS and SSTs may be more complex than the relationships between precipitation and SSTs described above.

To develop our empirical model of FSS, we used 2001–2009 fire counts detected by the Moderate Resolution Imaging Spectroradiometer (MODIS) onboard NASA's Terra satellite (*26*) along with Oceanic Niño Index (ONI) (*27*) and Atlantic Multidecadal Oscillation index (AMO) (*28*) SST anomaly time series (*29*). MODIS provides consistent information on active fires, with omission and commission errors quantified in past work using ground observations and higher-resolution satellite imagery [e.g., (*29*–*31*)]. To identify the optimal lead times for using ONI and AMO to predict fires, we separately calculated the correlation between MODIS-derived estimates of FSS and each of the two climate indices for different months prior to the peak fire month

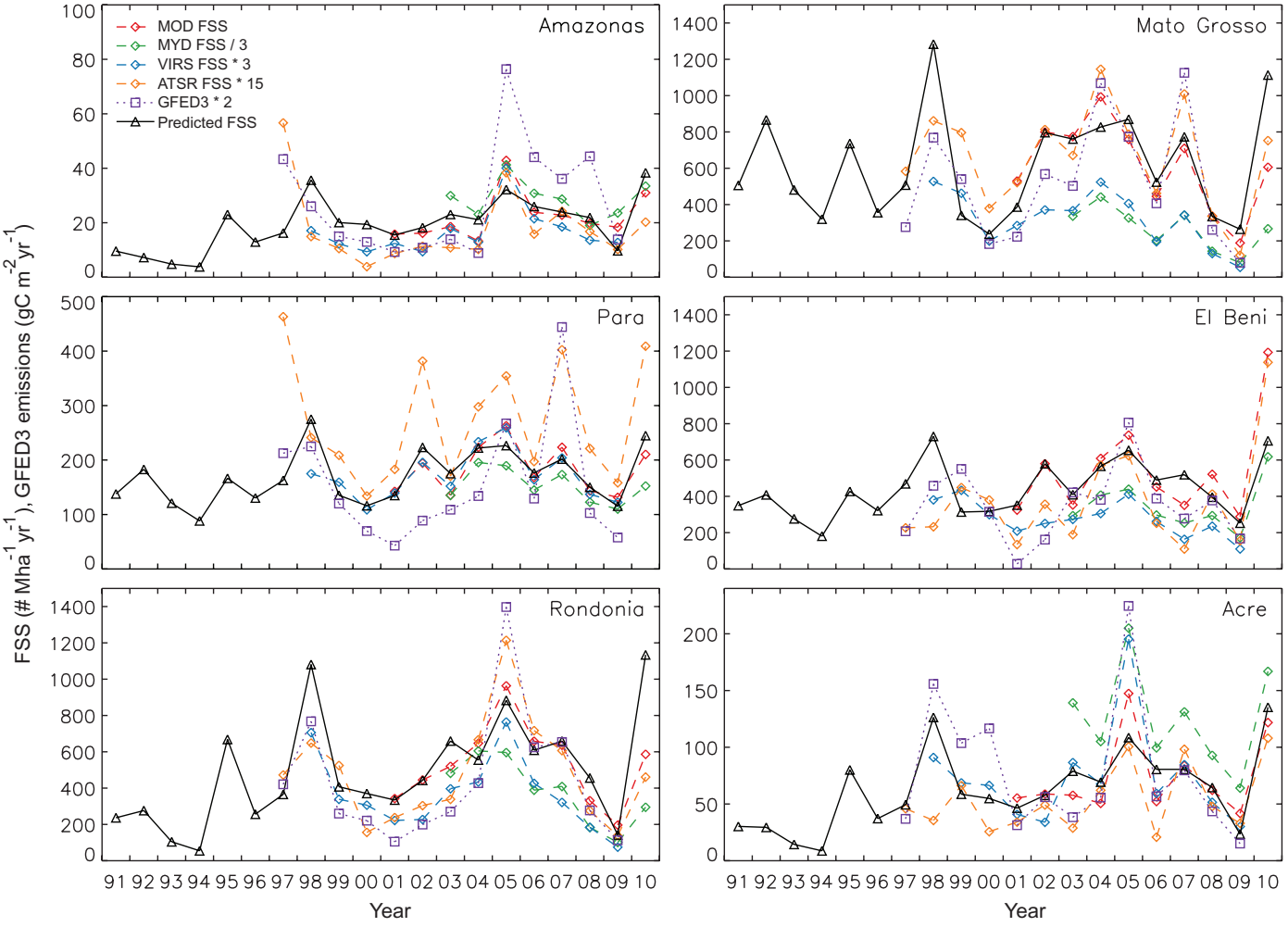

Fig. 2. Interannual variability of FSS from different satellites and carbon emissions from GFED3 compared to predictions from the empirical model (Eq. 1). The different satellite products are denoted as in Table 1. These FSS data sets are derived from satellite spectroradiometer observations of active fire counts with widely varying detector sensitivities and spatial resolutions, and therefore they are scaled to allow for more direct comparisons of interannual variability. The GFED3 fire carbon emissions estimates from 1997–2009 were scaled in each region except for Amazonas. Some of the variability in the observations not captured by our predictive model probably can be attributed to directional changes in land use within each region (*29*) (fig. S8).

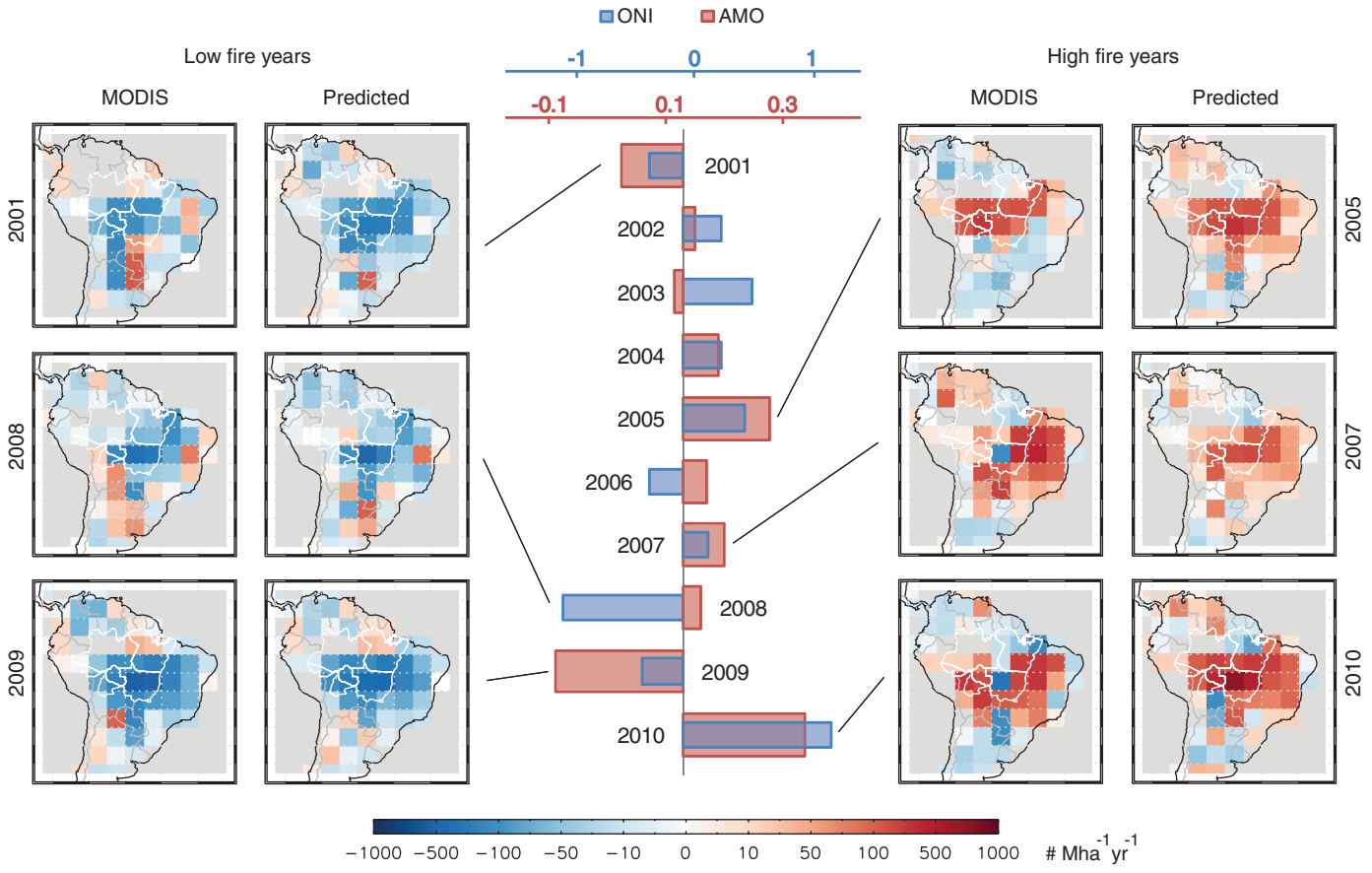

Fig. 3. FSS anomalies for selected years and their relationship to annual ONI and AMO. ONI and AMO were averaged during February to April, months with optimal leads for these two indices in high-fire states in Southern Hemisphere South America. Annual FSS anomalies observed by MODIS are shown relative to the 2001–2009 mean. Positive and negative anomalies in ONI and AMO also are shown relative to 2001–2009 mean values (−0.08 and 0.13 for ONI and AMO, respectively).

(i.e., for lead times of 1 to 10 months; defined relative to the end of the 3-month SST anomaly averaging interval of each climate index) in states of Brazil and Bolivia where biomass burning is high (Table 1 and fig. S1). We also estimated the optimal lead times for 5° × 5° regions across the continent (Fig. 1).

We defined our empirical predictive model as a linear combination of the two climate indices sampled during these months of maximum correlation:

$$\mathrm{FSS}_{\mathrm{predicted}}(x,t) = a(x) \times \mathrm{ONI}[t,m(x) - \tau_{\mathrm{ONI}}(x)] + b(x) \times \mathrm{AMO}[t,m(x) - \tau_{\mathrm{AMO}}(x)] + c(x) \quad (1)$$

where $\mathrm{FSS}_{\mathrm{predicted}}$ is the predicted FSS in region x and year t; a and b are spatially varying coefficients that represent the sensitivities of FSS in each region to ONI and AMO, respectively; and c is a constant. We obtained a, b, and c by fitting the observed time series of annual FSS from MODIS during 2001–2009 (Fig. 1C) with ONI and AMO during the same period. ONI and AMO were sampled each year during months with lead times τ_{ONI} and τ_{AMO} relative to the peak fire month (m) in each region. The lead times varied spatially in each state or 5° × 5° region according to the maximum correlation (either positive or negative) observed between FSS and the individual climate indices.

Fires in the eastern Amazon were more sensitive to ONI, whereas AMO had the largest impacts on FSS in the southern and southwestern Amazon (Fig. 1). The AMO influence on fires had a distinctive north-south pattern, with correlations switching from strongly positive to strongly negative north of the equator (Fig. 1 and fig. S2). AMO had a stronger positive correlation with FSS in Rondonia, Pará, El Beni, Amazonas, and Acre, whereas ONI was more closely linked with FSS in Mato Grosso (Table 1 and fig. S3). These spatial patterns were generally consistent with observed relationships between Pacific and Atlantic SST anomalies and precipitation variability within the Amazon (*20*).

Optimal lead times for the two climate indices relative to the peak fire month were 4 to 6 months for AMO and 3 to 7 months for ONI for states other than Amazonas (Table 1). By combining information from AMO and ONI in our empirical regression model (Eq. 1), we were able to explain some of the interannual variability in FSS across South America during 2001–2009 from MODIS (Fig. 1D). Notably, high-fire years in 2004, 2005, and 2007 had the highest values of AMO (and positive values of ONI) during the preceding January-to-March period (when lead times were optimal), whereas in the lowest-fire year (2009) AMO and ONI were both negative (fig. S4).

To verify the model, we compared the model predictions with MODIS FSS data from 2010 (this year was not used to develop the model), FSS data derived from three other satellites, and carbon emissions from the Global Fire Emissions Database version 3 (GFED3) (*9*) that integrates 500-m burned area and active fires from multiple sources during 1997–2009 (Fig. 2). The model predicted a considerable increase in fires in all regions in 2010 (relative to the 2008 and 2009 fire seasons) that was consistent with all of the available satellite observations (Fig. 2). Examination of the 2010 predictions in more detail for MODIS shows that the model generated reasonably accurate predictions for Acre and Pará; overestimated fires in Rondonia, Amazonas, and Mato Grosso; and underestimated fires in El Beni (fig. S5). Predictions from the model in the pre-MODIS era, relative to FSS data from other satellites and carbon emissions from GFED3, were

most robust for Rondonia and Mato Grosso (Fig. 2 and figs. S5 to S7). For these two states, residuals between observed and predicted FSS during 2001–2010 suggested that decreasing levels of deforestation during the second half of the decade reduced FSS and led to model overestimation of FSS in later years, indicating the influence of land use decisions affecting deforestation fires independent of climate (fig. S8).

The spatial patterns of high- and low-severity fire seasons across South America varied considerably and were partially captured by the model. In 2010, for example, the model predicted anomalously high levels of fire activity in both the southeastern and southwestern part of the Amazon basin, consistent with the observed pattern from MODIS (Fig. 3). In 2007, in contrast, both model estimates and MODIS observations indicated that anomalously high fires were distributed primarily in the southeastern part of the basin. These 2 years had high FSS despite the lowest deforestation rates during the study period.

Many different types of fire occur in tropical forest and savanna biomes, including deforestation fires, agricultural waste burning, and accidental forest and savanna fires from burning in adjacent agricultural areas. To examine the potential to develop separate forecasting models for these different fire types, we conducted three sensitivity analyses in which we separately considered forest and nonforest fires, persistent and nonpersistent forest fires (*6*), and understory fires (*29, 32*). Relative to our more general model, these models derived for different fire types within each state had mostly similar levels of performance and lead times (table S1 and figs. S1 and S9); thus, our approach may be broadly applicable for many fire types, including fires that contribute to forest degradation. We broadly define forest degradation here as decreases in tree density and the woody biomass of forests that are not directly associated with land clearing.

What are the mechanisms that enable fire season forecasts from SSTs with lead times of about 3 to 5 months for important biomass-burning regions in Southern Hemisphere South America? These time scales are considerably longer than expected for direct atmospheric circulation adjustments to SST anomalies. Further, although SST anomalies vary relatively slowly (and often have relatively long autocorrelation time scales), the relationship between SST anomalies and FSS becomes weaker with shorter lead times (fig. S1).

We hypothesize that precipitation levels during the preceding wet season and during the onset of the dry season in forests of Southern Hemisphere South America act as a key regulator of drought intensity during the subsequent dry season. Evidence supporting this hypothesis comes from analysis of the seasonal distribution of active fires during high- and low-fire years (fig. S10). For satellite observations available over the past decade, the midpoint of the fire season occurred earlier during high-fire years (fig. S11), likely as a consequence of reduced precipitation during the preceding months. This finding also is consistent with the observation that precipitation anomalies 1 to 4 months before the peak fire month (corresponding to the dry season and the wet-to-dry transition season) were more negatively correlated with the annual sum of fire counts than were precipitation anomalies during the peak fire month (fig. S12). The correlation between AMO and precipitation during the wet-to-dry transition period and early dry season was particularly strong for southwestern Amazonia (fig. S13). Patterns of interannual variability in precipitation also indicated that climate at the onset of the dry season was an important factor; standard deviations and coefficients of variation were higher during the wet-to-dry transition period than for the subsequent dry-to-wet transition (fig. S14).

One possible contributing factor for the time delays between SST anomalies and dry-season intensity may involve recharge of soil moisture in forests during the wet season. High SST anomalies in the North Atlantic from November to May limit the southward movement of the ITCZ and thus prevent a full recharge of soil moisture levels in forest ecosystems across the central and southern Amazon during these months (fig. S13). As a consequence, transpiration rates by trees may be reduced below average during the following dry season, with impacts for both surface humidity and precipitation (*3*). The time scales for these forest-mediated interactions are consistent with earlier work documenting deep rooting systems (*33*) and hydraulic redistribution (*34*) required to maintain high levels of evapotranspiration during the dry season (*35*). This mechanism also is consistent with climate model simulations indicating that shallower rooting depth parameterizations increase the vulnerability of tropical forests to future fire within the model (*14*).

Our results and earlier work by Fernandes *et al.* (*15*) provide evidence that Atlantic and Pacific SSTs may be used to predict FSS variability with lead times of 3 to 5 months in many regions of high biomass burning in South America. Interseasonal fire forecasts may allow for the design of more effective mitigation and adaptation strategies (*29*) and improve our understanding of how fires are likely to respond to changes in Pacific and Atlantic Ocean SSTs expected over the next several decades (*22*, *29*). Managing fires to conserve biodiversity and carbon stocks in forest and savanna ecosystems requires advance planning on multiple time scales, including the design of policy mechanisms that modify long-term development trajectories (*36*) as well as improved use of short-term meteorological forecasts of fire behavior during years with high FSS [e.g., (*37*)]. Our analysis suggests that interseasonal fire forecasts may complement fire management efforts on these shorter and longer time scales.

References and Notes

1. Y. Pan *et al.*, *Science* **333**, 988 (2011).
2. G. R. van der Werf *et al.*, *Nat. Geosci.* **2**, 737 (2009).
3. R. Ramos da Silva, D. Werth, R. Avissar, *J. Clim.* **21**, 1153 (2008).
4. J. Shukla, C. Nobre, P. Sellers, *Science* **247**, 1322 (1990).
5. M. A. Cochrane, *Nature* **421**, 913 (2003).
6. D. C. Morton *et al.*, *Glob. Change Biol.* **14**, 2262 (2008).
7. The Amazon Deforestation Monitoring Project (Programa de cálculo do desflorestamento da Amazônia—PRODES); data available at www.obt.inpe.br/prodes.
8. L. E. Aragão, Y. E. Shimabukuro, *Science* **328**, 1275 (2010).
9. G. R. van der Werf *et al.*, *Atmos. Chem. Phys.* **10**, 11707 (2010).
10. W. H. Li, R. Fu, R. E. Dickinson, *J. Geophys. Res.* **111**, D02111 (2006).
11. Y. Malhi *et al.*, *Proc. Natl. Acad. Sci. U.S.A.* **106**, 20610 (2009).
12. D. Nepstad *et al.*, *Glob. Change Biol.* **10**, 704 (2004).
13. R. A. Silvestrini *et al.*, *Ecol. Appl.* **21**, 1573 (2011).
14. N. Golding, R. Betts, *Global Biogeochem. Cycles* **22**, GB4007 (2008).
15. K. Fernandes *et al.*, *Geophys. Res. Lett.* **38**, L12701 (2011).
16. J. A. Marengo *et al.*, *J. Clim.* **21**, 495 (2008).
17. S. L. Lewis, P. M. Brando, O. L. Phillips, G. M. F. van der Heijden, D. Nepstad, *Science* **331**, 554 (2011).
18. L. E. Aragão *et al.*, *Philos. Trans. R. Soc. Ser. B* **363**, 1779 (2008).
19. J. Ronchail *et al.*, *Int. J. Climatol.* **22**, 1663 (2002).
20. J. H. Yoon, N. Zeng, *Clim. Dyn.* **34**, 249 (2010).
21. S. O. Los, G. J. Collatz, L. Bounoua, P. J. Sellers, C. J. Tucker, *J. Clim.* **14**, 1535 (2001).
22. V. E. Kousky, M. T. Kagano, I. F. A. Cavalcanti, *Tellus A* **36A**, 490 (1984).
23. C. F. Ropelewski, M. S. Halpert, *Mon. Weather Rev.* **115**, 1606 (1987).
24. N. Zeng *et al.*, *Environ. Res. Lett.* **3**, 014002 (2008).
25. P. M. Cox *et al.*, *Nature* **453**, 212 (2008).
26. C. O. Justice *et al.*, *Remote Sens. Environ.* **83**, 244 (2002).
27. K. E. Trenberth, *Bull. Am. Meteorol. Soc.* **78**, 2771 (1997).
28. K. E. Trenberth, D. J. Shea, *Geophys. Res. Lett.* **33**, L12704 (2006).
29. See supporting material on *Science* Online.
30. J. T. Morisette *et al.*, *Earth Interact.* **9**, 1 (2005).
31. W. Schroeder *et al.*, *Remote Sens. Environ.* **112**, 2711 (2008).
32. D. C. Morton *et al.*, *Remote Sens. Environ.* **115**, 1706 (2011).
33. D. C. Nepstad *et al.*, *Nature* **372**, 666 (1994).
34. J. E. Lee, R. S. Oliveira, T. E. Dawson, I. Fung, *Proc. Natl. Acad. Sci. U.S.A.* **102**, 17576 (2005).
35. H. R. da Rocha *et al.*, *Ecol. Appl.* **14**, S22 (2004).
36. B. S. Soares-Filho *et al.*, *Nature* **440**, 520 (2006).
37. Daily fire risk and weekly fire forecast maps for South America were developed by the Weather Forecasting and Climate Studies Center (CPTEC) in the National Institute for Space Research (INPE) of Brazil: http://sigma.cptec.inpe.br/queimadas/risco_eta.html.

Acknowledgments: Supported by NASA grants NNX08AF64G and NNX10AT83G. The GFED3 carbon emissions time series is publicly available at www.globalfiredata.org.

Supporting Online Material

www.sciencemag.org/cgi/content/full/334/6057/787/DC1
Materials and Methods
SOM Text
Figs. S1 to S15
Table S1
References

7 June 2011; accepted 21 September 2011
10.1126/science.1209472